Electronic Supplementary Information (ESI)

An aliphatic MOF with molecular sieving effect for efficient C_2H_2/C_2H_4 separation

Xianzhen Li,[a] Chen Cao[a], Ziwen Fan[a], Jianfa Liu[a], Tony Pham[b], Katherine A. Forrest[b] and Zheng Niu*[a]

[a] College of Chemistry, Chemical Engineering and Materials Science, Soochow University, Suzhou 215123, China.
[b] Department of Chemistry, University of South Florida, 4202 East Fowler Avenue, CHE 205A, Tampa, Florida 33620–5250, United States.

* Corresponding author.

E-mail: zhengniu@suda.edu.cn.

Table of Contents

1. General information

All other chemicals and reagents were commercially available and used without further purification. The IR spectra were recorded on a Varian 1000 FT-IR spectrometer as KBr disks in the range of 4000-400 cm^{-1}. The powder X-ray diffraction (PXRD) patterns were collected on a PANalytical Aeris diffractometer with Cu-Kα radiation (λ = 1.5406 Å) over the 2θ range of 3-50° at room temperature. The thermogravimetric analyses (TGA) were performed on a Mettler TGA/SDTA851 thermal analyzer under an N_2 atmosphere with a heating rate of 5 °C min^{-1}. The low-pressure gas sorption isotherms were collected on an ASAP 2020 Surface Area and Porosity Analyzer (Micromeritics) which equipped with a turbo molecular vacuum pump. The breakthrough experiment was monitored by gas chromatography analyzer (990 Micro GC, Agilent), and the test gas was a mixture of acetylene and ethylene.

1.2 Preparation of $Cu(bodc)(bpy)_{0.5}\cdot 2H_2O$ (SDMOF-1)

A mixture of bicyclo [2.2.2] octane-1,4-dicarboxylic acid (H_2bodc; 0.022 mmol, 4.36 mg) and bipyridine (bpy; 0.012 mmol, 1.87 mg) was dissolved in DMF (0.6 mL) and sonicated for 10 minutes. Cu $(NO_3)_2\cdot 3H_2O$ was dissolved in H_2O (1.2 mL) then added dropwise. After sonication for 30 minutes, hydrothermal tubes with the mixture were placed in the oven for programmed heat-up, which started at a rate of 12 °C/min, maintained at 100 °C for 48 h, and then cooled down at a rate of 6 °C/min. Finally, green crystals were obtained with a yield of 64 %. Anal. calcd. (%) for $C_{15}H_{16}CuNO_4$: C,53.32, H, 4.77, N, 4.15; found: C, 51.37, H, 4.67, N, 4.05. IR (KBr disk, cm^{-1}): 2957 (s), 2872 (s), 1608 (s), 1458 (m), 1405 (s), 1218(m), 1109 (m), 1039 (w), 864 (m), 809 (m), 755 (m), 634 (m).

1.3 Preparation of actived SDMOF-1

The crystals of $Cu(bodc)(bpy)_{0.5}\cdot 2H_2O$ were soaked in anhydrous methanol for 3 days with fresh methanol 6 times. Then, the crystals were vacuumed at room temperature till the pressure below to 5 μmHg, the temperature was increased to 140 °C and vacuum for 12 h. Consequently, the green crystal of anhydrous SDMOF-1 was obtained.

1.4 Preparation of SDMOF-1@C_2H_2

The selected activated SDMOF-1 was filled into a glass tube and collect with ASAP 2020, and the sample was vacuumed at 140 °C for 12 h. After the sample cooling down, the C_2H_2 gas was induced into the sample until the pressure reach to 1 bar at 298 K. The crystals were picked out and covered with the degassed oil in the glove box after 3 h for single crystal X-ray diffraction measurements.

2. Single-crystal X-ray diffraction crystallography

Single crystal with appropriate dimensions was chosen under an optical microscope and quickly coated with high vacuum grease to prevent decomposition. Crystallographic data of SDMOF-1 and C_2H_2 loaded SDMOF-1 were collected with a Bruker D8-Quest diffractometer with a graphite monochromated Ga Kα radiation (λ = 1.34138Å). The cell parameters refinement and data reduction were performed using the program Bruker Apex III with absorption correction (multi-scan) applied[1]. All the structures were solved by direct methods and refined anisotropically by full-matrix least-squares techniques based on F^2 using the SHELXS-97 and SHELXL-97 programs[2] contained on Olex 2[3]. Anisotropic thermal parameters were assigned to all non-hydrogen atoms. The hydrogen atoms of the ligand were generated geometrically; the hydrogen atoms of the C_2H_2 molecules were in Fourier-difference electron density maps and refined with isotropic temperature factors. The large solvent accessible void in the lattice is caused by the vacuum process before single crystal diffraction measurement. Pertinent crystallographic data collection and refinement parameters are collated in **Table S1** and **S2**. Crystallographic data have been deposited in the Cambridge Crystallographic Data Center (CCDC) with the reference numbers of 2260960 for **SDMOF-1**, and 2260961 for **SDMOF-1@C_2H_2**.

3. Low-pressure gas adsorption measurement.

Crystalline samples (50-60 mg) of activated SDMOF-1 were transferred to a pre-weighed 6-mm large bulb glass sample cell. The low-pressure gas sorption isotherms were collected on an ASAP 2020 Surface Area and Porosity Analyzer (Micromeritics) which equipped with a turbo molecular vacuum pump. The apparent surface areas of activated SDMOF-1 were determined from the nitrogen adsorption isotherm collected at 77 K and carbon dioxide adsorption isotherm collected at 195 K by applying the Brunauer-Emmett-Teller (BET) and Langmuir models.

4. Ideal Adsorbed Solution Theory

The C_2H_2/C_2H_4 selectivities for the adsorbate mixture compositions of interest (1:99) in SDMOF-1 at 298 K were calculated using ideal adsorbed solution theory (IAST)[4].The single-component isotherms for C_2H_2 and C_2H_4 at 298 K were fitted to the dual-site Langmuir-Freundlich equation (DSLF) equation[5]:

$$n(P) = \frac{nm_1 b_1 P^{\left(\frac{1}{t_1}\right)}}{1 + b_1 P^{\left(\frac{1}{t_1}\right)}} + \frac{nm_2 b_2 P^{\left(\frac{1}{t_2}\right)}}{1 + b_1 P^{\left(\frac{1}{t_2}\right)}} \quad (1)$$

In this equation, n is the amount adsorbed per mass of material (in mmol g^{-1}), P is the total pressure (in kPa) of the bulk gas at equilibrium with the adsorbed phase, n_{m1}

and n_{m2} are the saturation uptakes (in mmol g^{-1}) for sites 1 and 2, b_1 and b_2 are the affinity coefficients (in kPa^{-1}) for sites 1 and 2, and t_1 and t_2 represent the deviations from the ideal homogeneous surface (unitless) for sites 1 and 2. The parameters that were obtained from the fitting are found in **Tables S3 and S4**. Both isotherms were fitted with $R^2 > 0.9999$. Next, the spreading pressure for adsorbates *i* and *j* can be calculated using the following equations:

$$\frac{\pi_i^0 A}{RT} = \int_0^{P_i^0(\pi)} \frac{n_i(P)}{P} dP \tag{2}$$

$$\frac{\pi_j^0 A}{RT} = \int_0^{P_j^0(\pi)} \frac{n_j(P)}{P} dP \tag{3}$$

In the above equations, *A* represents the specific surface area (assumed to be the same for all adsorbates), *R* is the ideal gas constant, *T* is the temperature, and $P°_i(\pi)$ and $P°_j(\pi)$ are the equilibrium gas phase pressures corresponding to the solution temperature and solution spreading pressure for the sorption of pure components *i* and *j*, respectively. Further, the following equations hold true for a two-component mixture according to IAST:

$$\pi_i^0 = \pi_j^0 \tag{4}$$

$$P y_i = P_i^0 x_i \tag{5}$$

$$P y_j = P_j^0 x_j \tag{6}$$

$$x_i + x_j = 1 \tag{7}$$

$$y_i + y_j = 1 \tag{8}$$

Here, x_i and x_j are the mole fractions of components *i* and *j*, respectively, in the adsorbed phase, and y_i and y_j are the mole fractions of components *i* and *j*, respectively, in the gas phase. The previous seven equations are seven independent equations with nine unknowns. In order to solve for all of the unknowns, two quantities must be specified, particularly *P* and y_i. Utilization of the equations yield the following equilibrium expression for adsorbates *i* and *j*:

$$\int_0^{\frac{Py_i}{x_i}} \frac{n_i(P)}{P} dP = \int_0^{\frac{P(1-y_i)}{(1-x_i)}} \frac{n_j(P)}{P} dP \quad (9)$$

The above equation was solved for x_i using numerical analysis for a range of pressures at a specified y_i value. Finally, the selectivity for adsorbate *i* relative to adsorbate *j* was calculated using the following:

$$S_{i/j} = \frac{x_i y_j}{x_j y_i} \quad (10)$$

The total amount of gas adsorbed within the mixture can be calculated using the following equation:

$$n_{tot} = \frac{n_i^0(P_i^0) n_j^0(P_j^0)}{x_i n_j^0(P_j^0) + x_j n_i^0(P_i^0)} \quad (11)$$

Where $n°_i(P°_i)$ and $n°_j(P°_j)$ are the amount adsorbed in the standard state at the equilibrium gas phase pressure for sorbates *i* and *j*, respectively. The actual amount adsorbed for each component within the mixture can be calculated using the following:

$$n_i = n_{tot} x_i \quad (12)$$

$$n_j = n_{tot} x_j \quad (13)$$

5. The separation potential (ΔQ)

For separation of a binary mixture of components A and B, the adsorption selectivity, $S_{A/B}$, is defined by:

$$S_{A/B} = \frac{q_A/q_B}{y_A/y_B} \quad (14)$$

Where q_A, q_B are the molar loadings (units: mol kg $^{-1}$) in the adsorbed phase in equilibrium with a bulk gas phase mixture with mole fractions y_A, and $y_B = 1 - y_A$. The volumetric uptake capacities are:

$$Q_A = \rho q_A \quad (15)$$

$$Q_B = \rho q_B \tag{16}$$

Where ρ is the crystal framework density of the MOF, expressed say in units of kg m^{-3}, or kg L^{-1}. The uptake capacities can be calculated using pure components isotherm fits, along with the mixed-gas Langmuir model or the Ideal Adsorbed Solution Theory (IAST) of Myers and Prausnitz for adsorption equilibrium.

Using the shock wave model for fixed bed adsorbers, Krishna[6, 7] has suggested that the appropriate metric is the separation potential, ΔQ. The appropriate expression describing the productivity of pure C_2H_4 in the desorption phase of fixed-bed operations is:

$$\Delta Q = Q_A \frac{y_B}{1 - y_B} - Q_B \tag{17}$$

The mole fraction y_B refers to composition of the feed mixture.

6. Theory Isosteric Heat of Adsorption

The experimental isosteric heat of adsorption (Q_{st}) values for C_2H_2 and C_2H_4 in SDMOF-1 were determined by first fitting the adsorption isotherms at 273 and 298 K for the respective adsorbates to the DSLF equation (see Ideal Adsorbed Solution Theory section above) and subsequently applying the Clausius-Clapeyron method[8].The parameters that were obtained from the fitting of the C_2H_2 and C_2H_4 adsorption isotherms are found in **Tables S3 and S4**. All isotherms were fitted with $R^2 > 0.999$.

The fitted parameters were used to calculate the Q_{st} values for a range of uptakes through the Clausius-Clapeyron equation, which is the following:

$$Q_{st} = -R \frac{\partial \ln P}{\partial \left(\frac{1}{T}\right)} \tag{14}$$

where T is the temperature (in K) and R is the ideal gas constant. The partial derivative term actually represents the slope of the plot of ln P vs. $1/T$ for a number of isotherms at different temperatures at various loadings. Therefore, the above Q_{st} equation can be simplified to:

$$Q_{st} = -mR \tag{15}$$

where m is the slope, which can be calculated by the following for two different temperatures and their corresponding pressures:

$$m = \frac{T_1 T_2}{T_1 - T_2} \ln\left(\frac{P_2}{P_1}\right) \quad (16)$$

where $P_2 > P_1$ and $T_2 > T_1$. The P_i values were back-calculated for a range of uptakes using the DSLF equation *via* an iterative technique (e.g., the Newton-Raphson method)[9].

7. Periodic Density Functional Theory

The binding energy for C_2H_2 in SDMOF-1 was determined using the experimental single X-ray crystal structure in which all C_2H_2 molecules were resolved at the primary binding sites in the material. Periodic density functional theory (DFT) calculations were performed with only one C_2H_2 molecule localized at the primary binding site within a single unit cell of the MOF. A full structural relaxation was performed on this system in which the atomic positions were permitted to fluctuate, but with the basis vectors held constant. After the relaxation, counterpoise-corrected energies of the MOF and adsorbate components were individually determined and subtracted from the total system energy to yield a binding energy of -55.46 kJ mol^{-1}. These calculations were implemented with the CP2K simulation package[10] using MOLOPT basis sets at the triple ζ level of theory[11, 12], Perdew–Burke–Ernzerhof (PBE) pseudopotentials[13, 14], and DFT-D pairwise dispersion corrections[15].

8. Breakthrough test

Dynamic breakthrough experiments were carried out in the dynamic gas breakthrough equipment with gas mixing system and online gas chromatography system. The activated sample was packed in a stainless-steel column (4.6 mm inner diameter × 50 mm). The weight of sample SDMOF-1 powder packed in the column was 0.52 g. The column packed with the sample was firstly activated with He flow (12 mL min^{-1}) for 1 h at room temperature (298 K). After preparation, the mixed gas (C_2H_2/C_2H_4: 1/99, v/v) flow was introduced around 7 mL min^{-1} into these columns. Outlet gas from the column was monitored using gas chromatography (990 Micro GC, Agilent). The experimental set-up of the column breakthrough experiment is presented in **Figure S1**.

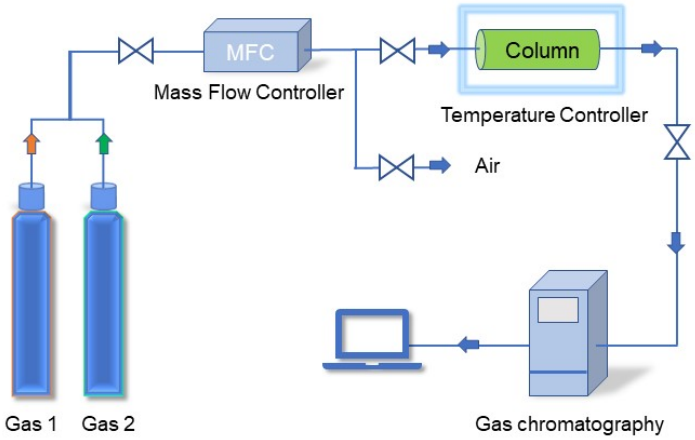

Figure S1 Schematic representation of the column breakthrough experiment set-up combined with the mass spectrophotometer.

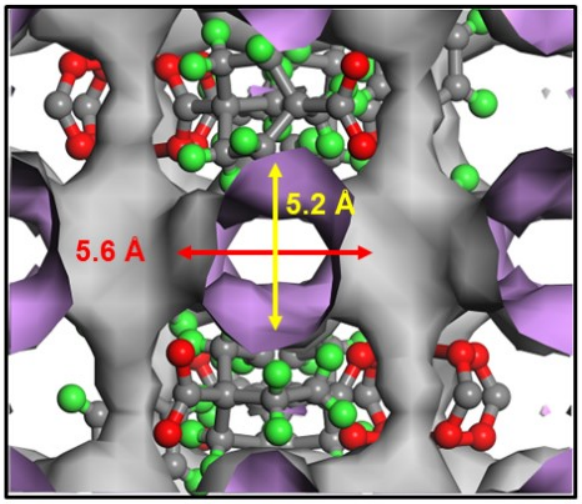

Figure S2 Cavity geometry and dimensions of as-synthesized SDMOF-1.

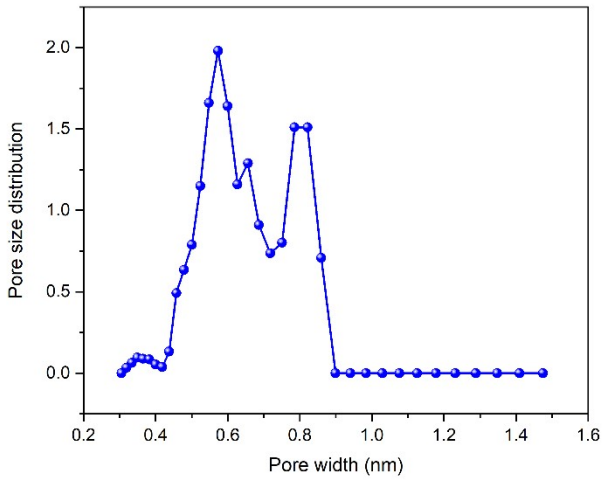

Figure S3 Pore size distribution (PSD) of SDMOF-1.

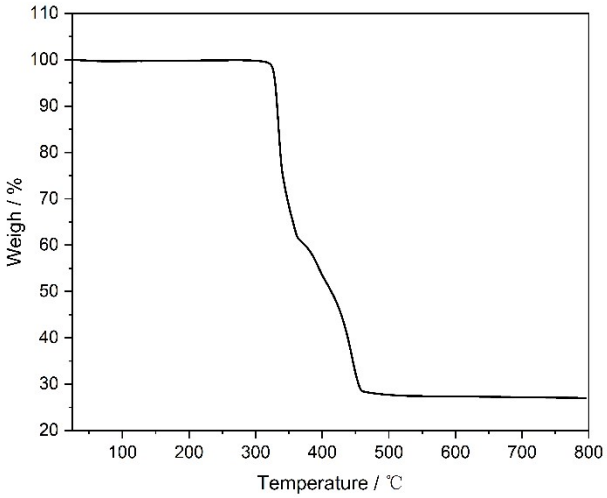

Figure S4 TGA curve of SDMOF-1. The samples were pretreated before thermogravimetric analysis and the water molecules contained in the structure were removed through heating. From 325 to 650 °C, SDMOF-1 gradually decomposed to CuO (observed value of weight loss: 27.1%, calculated value: 23.7%).

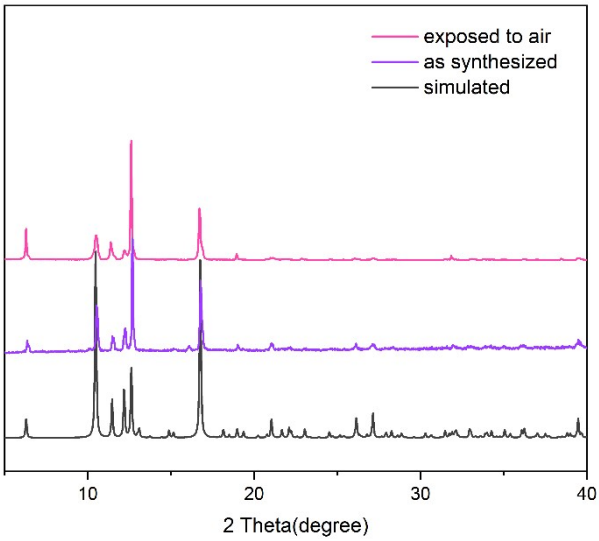

Figure S5 PXRD patterns of SDMOF-1. The pink line presented the PXRD pattern of SDMOF-1 exposed to the air for six months and the purple line presented the PXRD pattern of synthesized SDMOF-1.

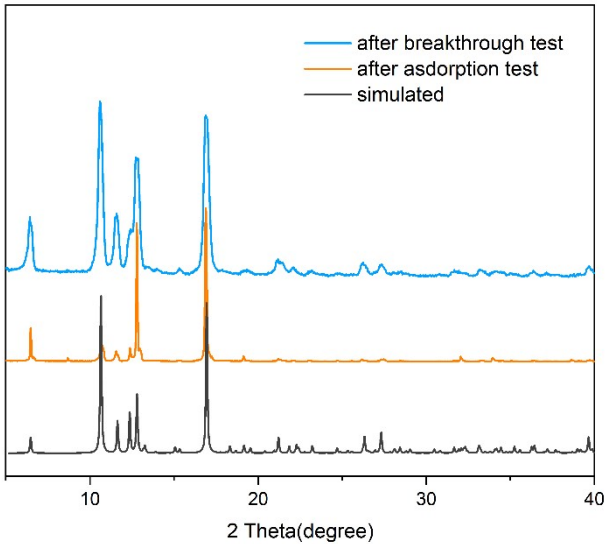

Figure S6 PXRD patterns of SDMOF-1 after breakthough test (blue line) and asdorption test (orange line).

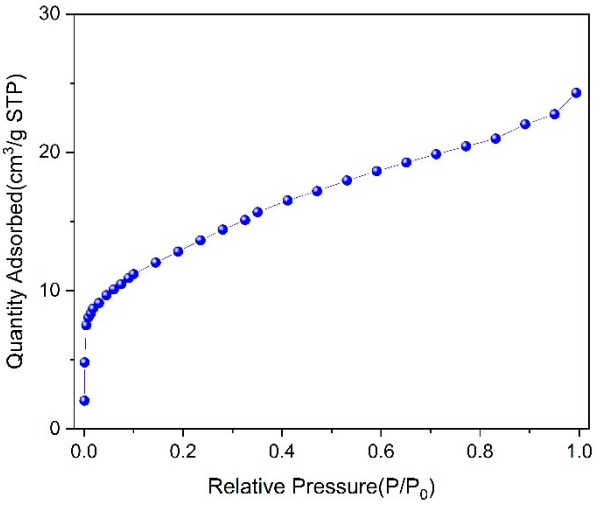

Figure S7 N_2 adsorption isotherm for SDMOF-1 at 77 K.

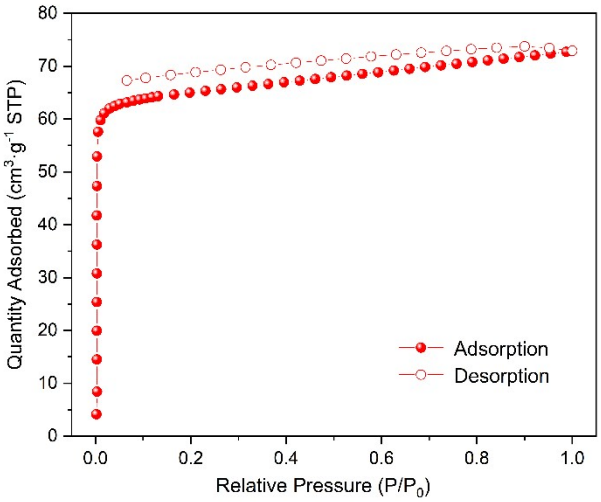

Figure S8 CO_2 adsorption isotherm for SDMOF-1 at 195 K.

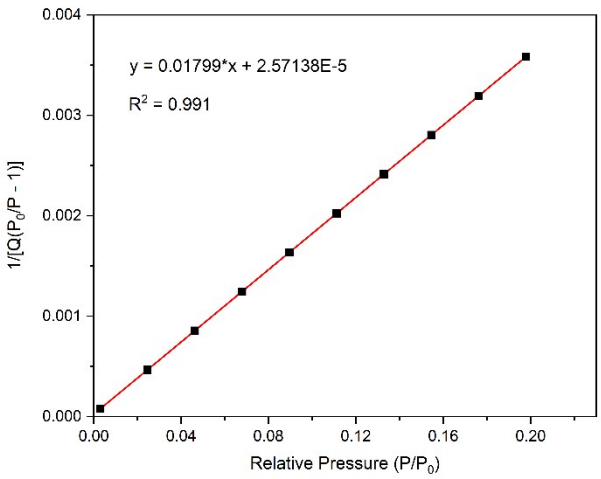

Figure S9 BET calculation based on CO_2 adsorption isotherm of SDMOF-1 at 195 K. (Standard Deviation: 2.57138 ± 2.92066E-5； 0.01799 ± 3.82803E-4).

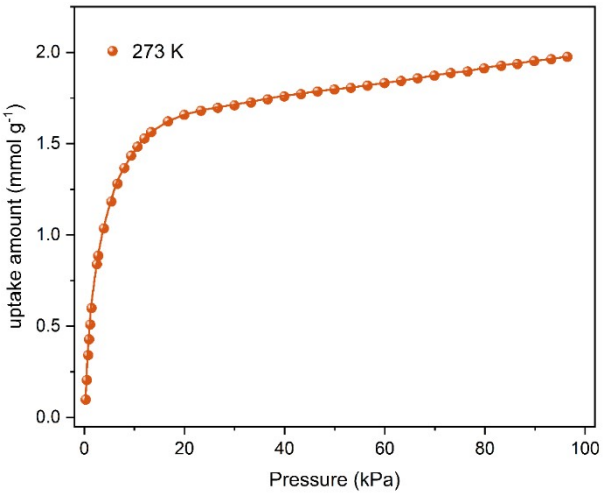

Figure S10 C_2H_2 adsorption isotherm of SDMOF-1 at 273 K (circles stand for experiment data; lines are from DSFL fitting).

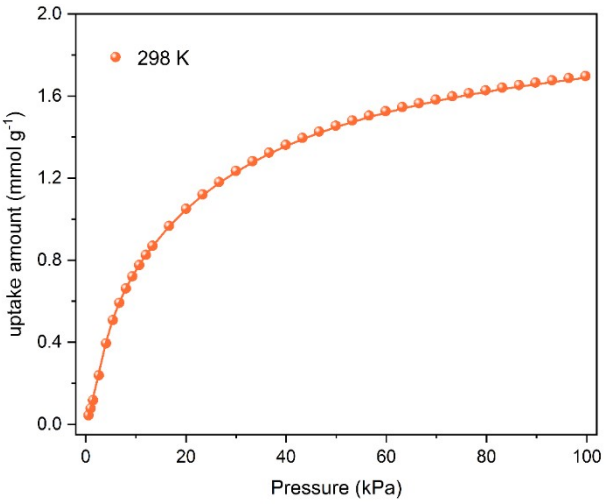

Figure S11 C_2H_2 adsorption isotherm of SDMOF-1 at 298 K (circles stand for experiment data; lines are from DSFL fitting).

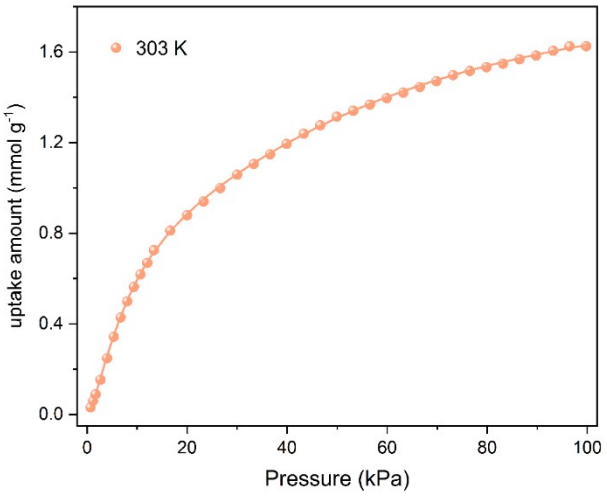

Figure S12 C_2H_2 adsorption isotherm of SDMOF-1 at 303 K (circles stand for experiment data; lines are from DSFL fitting).

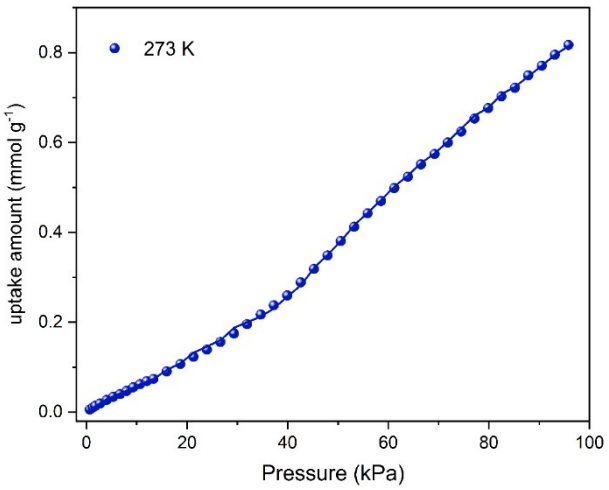

Figure S13 C_2H_4 adsorption isotherm of SDMOF-1 at 273 K (circles stand for experiment data; lines are from DSFL fitting).

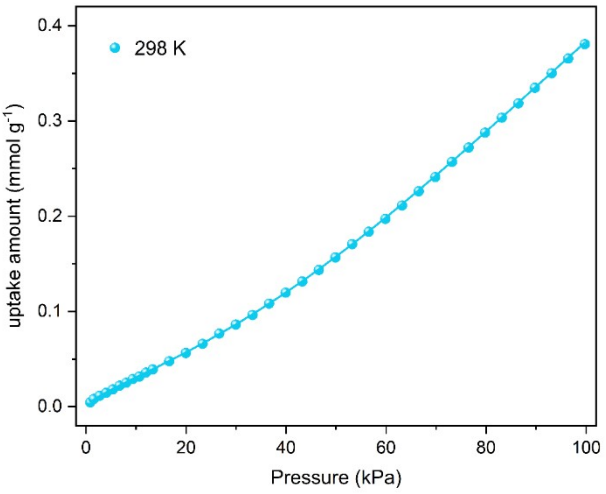

Figure S14 C_2H_4 adsorption isotherm of SDMOF-1 at 298 K (circles stand for experiment data; lines are from DSFL fitting).

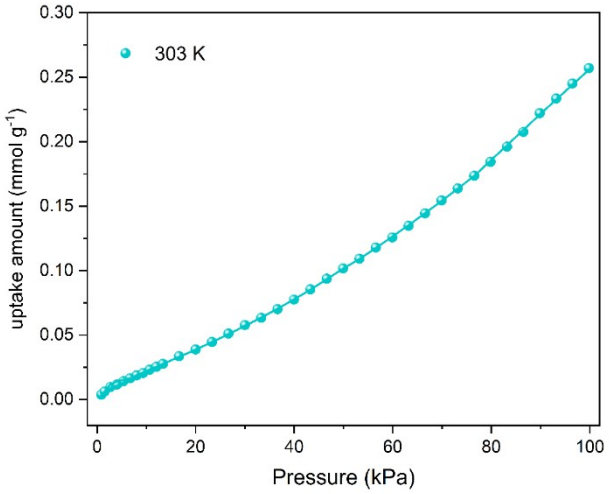

Figure S15 C_2H_4 adsorption isotherm of SDMOF-1 at 303 K (circles stand for experiment data; lines are from DSFL fitting).

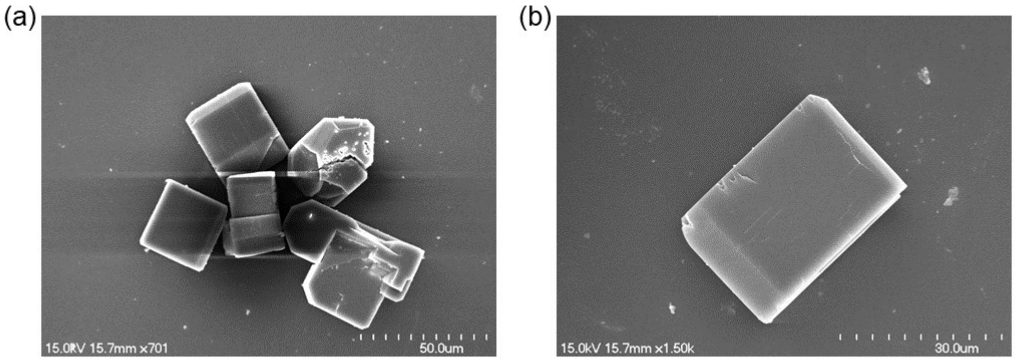

Figure S16 Scanning electron microscope (SEM) images of SDMOF-1 crystal.

Table S1 Crystal data and structure refinement parameters for SDMOF-1.

SDMOF-1	
Empirical formula	$C_{15}H_{20}CuNO_6$
CCDC number	2260960
Formula weight	373.86
Temperature [K]	120.00
Crystal system	orthorhombic
Space group (number)	$Pcca$ (54)
a [Å]	14.5103(10)
b [Å]	14.0161(9)
c [Å]	15.4240(10)
α [°]	90
β [°]	90
γ [°]	90
Volume [Å^3]	3136.9(4)
Z	8
ρ_{calc} [gcm^{-3}]	1.583
μ [mm^{-1}]	7.689
F(000)	1552
Crystal size [mm^3]	0.13×0.1×0.08
Crystal colour	blue
Crystal shape	block
Radiation	GaK_α (λ=1.34138 Å)
2Θ range [°]	9.12 to 116.19 (0.79 Å)
Index ranges	-18 ≤ h ≤ 18 -16 ≤ k ≤ 17 -19 ≤ l ≤ 19
Reflections collected	34607
Independent reflections	3294 R_{int} = 0.0861 R_{sigma} = 0.0525
Completeness to Θ = 53.594°	98.5 %

Data / Restraints / Parameters	3294/159/218
Goodness-of-fit on F^2	1.119
Final R indexes [$I \geq 2\sigma(I)$]	R_1 = 0.0895 wR_2 = 0.2169
Final R indexes [all data]	R_1 = 0.0980 wR_2 = 0.2204
Largest peak/hole [eÅ^{-3}]	1.30/-1.56

Table S2 Crystal data and structure refinement parameters for SDMOF-1@C_2H_2.

SDMOF-1@C_2H_2	
Empirical formula	$C_{31}H_{33}Cu_2N_2O_8$
CCDC number	2260961
Formula weight	688.67
Temperature [K]	120.00
Crystal system	orthorhombic
Space group (number)	$Ibca$ (73)
a [Å]	14.429(3)
b [Å]	15.544(3)
c [Å]	28.110(5)
α [°]	90
β [°]	90
γ [°]	90
Volume [Å^3]	6305(2)
Z	8
ρ_{calc} [gcm^{-3}]	1.451
μ [mm^{-1}]	7.572
F(000)	2840
Crystal size [mm^3]	0.15×0.12×0.1
Crystal colour	blue
Crystal shape	block
Radiation	GaK_α (λ=1.34139 Å)

2Θ range [°]	5.47 to 121.25 (0.77 Å)
Index ranges	-13 ≤ h ≤ 18 -20 ≤ k ≤ 11 -36 ≤ l ≤ 35
Reflections collected	13404
Independent reflections	3321 R_{int} = 0.0624 R_{sigma} = 0.0493
Completeness to Θ = 53.594°	90.7 %
Data / Restraints / Parameters	3321/1/202
Goodness-of-fit on F^2	1.092
Final R indexes [$I \geq 2\sigma(I)$]	R_1 = 0.0408 wR_2 = 0.1157
Final R indexes [all data]	R_1 = 0.0483 wR_2 = 0.1204
Largest peak/hole [eÅ^{-3}]	0.71/-0.71

Table S3 The fitted parameters for the dual-site Langmuir-Freundlich equation for the single component isotherms of C_2H_2 in SDMOF-1 at 273 K and 298 K.

	273 K	298 K
n_{m1}(mmol g^{-1})	4.666716152	0.987630639
n_{m2}(mmol g^{-1})	1.05410969	3.079531197
b_1(kPa^{-1})	9.24118E-10	0.042702805
b_2(kPa^{-1})	0.303380337	0.019085905
t_1	0.24030441	1.84741693
t_2	1.872492361	0.217983719
R^2	0.9999	0.9999

Table S4 The fitted parameters for the dual-site Langmuir-Freundlich equation for the single component isotherms of C_2H_4 in SDMOF-1 at 273 K and 298 K.

	273 K	298 K
n_{m1}(mmol g^{-1})	1.409535862	0.749786007
n_{m2}(mmol g^{-1})	2.425719243	2.219360343
b_1(kPa^{-1})	0.10127739	0.000644608
b_2(kPa^{-1})	2.73138E-05	1.46561E-05
t_1	0.065198862	7.944606589
t_2	1.170786369	0.780094155
R^2	0.9999	0.9999

Table S5 Summary of the adsorption uptakes, uptake radio, selectivities and heat of adsorption data for C_2H_2 and C_2H_4 in various MOFs.

MOFs	C_2H_2 uptake at 1.0 bar (mmol g^{-1})	C_2H_4 uptake at 1.0 bar (mmol g^{-1})	C_2H_2/C_2H_4 uptake ratio	Selectivity C_2H_2/C_2H_4 (1/99)	Q_{st} (C_2H_2, kJ mol^{-1})	Ref
SDMOF-1	1.7	0.38	4.47	26	47.5	This work
UPC-22	1.67	1.08	1.55	2.7	21.1	[16]
BSF-4	2.38	1.56	1.53	7.3	35	[17]
NCU-100a	4.57	0.32	14.3	7291.3	60.5	[18]
UTSA-200a	3.65	0.63	5.79	6320	40	[19]
ZU-33	3.77	0.7	5.39	1100	43.6	[20]
M´MOF-3a	1.9	0.4	4.75	24.03	25	[21]
APPT-Cd-ClO4$^-$	1.75	0.44	4.01	14.61	28.6	[22]
ZU-62-Ni	3	0.8	3.75	37.2	43	[23]
UTSA-100a	4.27	1.66	2.57	10.72	22	[24]

ELM-12	2.56	1	2.56	14.8	25.4	[25]
SIFSIX-1-Cu	8.5	4.11	2.07	10.63	30	[26]
SIFSIX-2-Cu	5.38	2.02	2.66	6.0	26.3	[26]
SIFSIX-2-Cu-i	4	2.2	1.82	44.8	52.9	[26]
SIFSIX-3-Ni	3.30	1.75	1.89	5.03	30.5	[27]
NUM-12a	5.37	3	1.79	1.4	38.1	[28]
NOTT-300	6.34	4.28	1.48	2.17	32	[29]
NKMOF-1-Ni	2.72	2.11	1.29	1272.6	60.3	[30]
CuI-MOF	1.25	1.03	1.22	1.4	21.4	[31]
ZJU-74a	3.8	3.21	1.18	24.2	45	[32]
Fe-MOF-74	6.8	6.1	1.11	2.08	46	[33]

Table S6 Summary of the breakthrough time for five times.

Cycle time	C_2H_2 breakthrough time (minutes)
1	20.69
2	22.41
3	22.41
4	20.69
5	19.83

References

1 A. Dawson, D. R. Allan, S. Parsons and M. Ruf, *J. Appl. Crystallogr.*, 2004, **37**, 410-416.

2 G. M. Sheldrick, *Acta Crystallogr. Sect. C-Struct. Chem.*, 2015, **71**, 3-8.

3 J. Lubben, C. M. Wandtke, C. B. Hubschle, M. Ruf, G. M. Sheldrick and B. Dittrich, *Acta Crystallogr A*, 2019, **75**, 50-62.

4 A. L. Myers and J. M. Prausnitz, *AlChE J.*, 1965, **11**, 121-127.
5 R. Babarao, Z. Q. Hu, J. W. Jiang, S. Chempath and S. I. Sandler, *Langmuir*, 2007, **23**, 659-666.
6 R. Krishna, *RSC Advances*, 2017, **7**, 35724-35737.
7 R. Krishna, *Sep. Purif. Technol.*, 2018, **194**, 281-300.
8 S. Chowdhury, R. Mishra, P. Saha and P. Kushwaha, *Desalination*, 2011, **265**, 159-168.
9 H. Pan, J. A. Ritter and P. B. Balbuena, *Langmuir*, 1998, **14**, 6323-6327.
10 T. D. Kühne, M. Iannuzzi, M. Del Ben, V. V. Rybkin, P. Seewald, F. Stein, T. Laino, R. Z. Khaliullin, O. Schütt, F. Schiffmann, D. Golze, J. Wilhelm, S. Chulkov, M. H. Bani-Hashemian, V. Weber, U. Borštnik, M. Taillefumier, A. S. Jakobovits, A. Lazzaro, H. Pabst, T. Müller, R. Schade, M. Guidon, S. Andermatt, N. Holmberg, G. K. Schenter, A. Hehn, A. Bussy, F. Belleflamme, G. Tabacchi, A. Glöß, M. Lass, I. Bethune, C. J. Mundy, C. Plessl, M. Watkins, J. VandeVondele, M. Krack and J. Hutter, *The Journal of Chemical Physics*, 2020, **152**, 194103.
11 J. VandeVondele and J. Hutter, *The Journal of Chemical Physics*, 2003, **118**, 4365-4369.
12 J. VandeVondele and J. Hutter, *The Journal of Chemical Physics*, 2007, **127**, 114105.
13 J. P. Perdew, K. Burke and M. Ernzerhof, *Phys. Rev. Lett.*, 1996, **77**, 3865-3868.
14 J. P. Perdew, K. Burke and M. Ernzerhof, *Phys. Rev. Lett.*, 1997, **78**, 1396-1396.
15 S. Grimme, J. Antony, S. Ehrlich and H. Krieg, *The Journal of Chemical Physics*, 2010, **132**, 154104.
16 X. P. Liu, Y. Li, C. L. Hao, W. D. Fan, W. Liu, J. Q. Liu and Y. J. Wang, *Inorg. Chem. Front.*, 2023, **10**, 824-831.
17 Y. B. Zhang, L. Y. Wang, J. B. Hu, S. Duttwyler, X. L. Cui and H. B. Xing, *CrystEngComm*, 2020, **22**, 2649-2655.
18 J. Wang, Y. Zhang, P. X. Zhang, J. B. Hu, R. B. Lin, Q. Deng, Z. L. Zeng, H. B. Xing, S. G. Deng and B. L. Chen, *J. Am. Chem. Soc.*, 2020, **142**, 9744-9751.
19 B. Li, X. L. Cui, D. O'nolan, H. M. Wen, M. D. Jiang, R. Krishna, H. Wu, R. B. Lin, Y. S. Chen, D. Q. Yuan, H. B. Xing, W. Zhou, Q. L. Ren, G. D. Qian, M. J. Zaworotko and B. L. Chen, *Adv. Mater.*, 2017, **29**, 1704210.
20 Q. Wang, J. Hu, L. Yang, Z. Zhang, T. Ke, X. Cui and H. Xing, *Nat. Commun.*, 2022, **13**, 2955.
21 S. C. Xiang, Z. J. Zhang, C. G. Zhao, K. L. Hong, X. B. Zhao, D. R. Ding, M. H. Xie, C. D. Wu, M. C. Das, R. Gill, K. M. Thomas and B. L. Chen, *Nat. Commun.*, 2011, **2**, 204.
22 G. X. Jin, X. Niu, J. Wang, J. P. Ma, T. L. Hu and Y. B. Dong, *Chem. Mater.*, 2018, **30**, 7433-7437.
23 L. F. Yang, A. Y. Jin, L. S. Ge, X. L. Cui and H. B. Xing, *Chem. Commun.*, 2019, **55**, 5001-5004.
24 T. L. Hu, H. L. Wang, B. Li, R. Krishna, H. Wu, W. Zhou, Y. F. Zhao, Y. Han, X. Wang, W. D. Zhu, Z. Z. Yao, S. C. Xiang and B. L. Chen, *Nat. Commun.*, 2015,

6, 7328.
25 L. B. Li, R. B. Lin, R. Krishna, X. Q. Wang, B. Li, H. Wu, J. P. Li, W. Zhou and B. L. Chen, *J. Mater. Chem. A*, 2017, **5**, 18984-18988.
26 X. L. Cui, K. J. Chen, H. B. Xing, Q. W. Yang, R. Krishna, Z. B. Bao, H. Wu, W. Zhou, X. L. Dong, Y. Han, B. Li, Q. L. Ren, M. J. Zaworotko and B. L. Chen, *Science*, 2016, **353**, 141-144.
27 J. Y. Zheng, X. L. Cui, Q. W. Yang, Q. L. Ren, Y. W. Yang and H. B. Xing, *Chem. Eng. J.*, 2018, **354**, 1075-1082.
28 Q. Zhang, S. Q. Yang, L. Zhou, L. Yu, Z. F. Li, Y. J. Zhai and T. L. Hu, *Inorg. Chem.*, 2021, **60**, 19328-19335.
29 S. H. Yang, A. J. Ramirez Cuesta, R. Newby, V. Garcia Sakai, P. Manuel, S. K. Callear, S. I. Campbell, C. C. Tang and M. Schröder, *Nat. Chem.*, 2015, **7**, 121-129.
30 Y. L. Peng, T. Pham, P. Li, T. Wang, Y. Chen, K. J. Chen, K. A. Forrest, B. Space, P. Cheng, M. J. Zaworotko and Z. Zhang, *Angew. Chem. Int. Ed.*, 2018, **57**, 10971-10975.
31 G. X. Jin, J. Wang, J. Y. Liu, J. P. Ma and Y. B. Dong, *Inorg. Chem.*, 2018, **57**, 6218-6221.
32 J. Pei, K. Shao, J. X. Wang, H. M. Wen, Y. Yang, Y. Cui, R. Krishna, B. Li and G. D. Qian, *Adv. Mater.*, 2020, **32**, e1908275.
33 Y. B. He, R. Krishna and B. L. Chen, *Energy Environ. Sci.*, 2012, **5**, 9107.